Progress in Physics of Applied Materials 6 (2026), Serial Number 12, 193-204

Semnan University

Progress in Physics of Applied Materials

journal homepage: https://ppam.semnan.ac.ir/

PC1D Modelling of the Impact of Layer Thickness, Doping Concentration, and Operating Temperature on InGaN Solar Cells

Nur Syahirah Khairuddin[a], Mohd Zaki Mohd Yusoff[a,b,c*], Hanim Hussin[d]

[a]*School of Physics and Material Studies, Faculty of Applied Sciences, Universiti Teknologi MARA, 40450 Shah Alam, Selangor, Malaysia*
[b]*Institute for Biodiversity and Sustainable Development (IBSD), Universiti Teknologi MARA, 40450 Shah Alam, Selangor, Malaysia*
[c]*Institute of Sciences (IOS), Universiti Teknologi MARA, 40450 Shah Alam, Selangor, Malaysia*
[d]*School of Electrical Engineering, College of Engineering, Universiti Teknologi MARA, 40450 Shah Alam, Selangor, Malaysia*

ARTICLE INFO

Article history:
Received: 2 November 2025
Revised: 1 January 2026
Accepted: 3 January 2026
Published online: 14 January 2026

Keywords:
InGaN;
GaN;
Si;
Quantum efficiency;
PC1D.

ABSTRACT

In this research, indium gallium nitride (InGaN), gallium nitride (GaN), and silicon (Si) were combined to develop a heterojunction solar cell with optimal results using the Personal Computer One Dimensional (PC1D) simulation. This research investigates the impact of structural and design parameters, specifically; thickness and doping, on the performance of InGaN solar cells. The electrical properties of these solar cells were examined to determine their optimum conditions. Based on the findings, appropriate layer thickness, doping concentration, and operation temperature, all together contribute to enhance electron mobility and solar cell efficiency (η). The quantum efficiency at the highest temperature is the lowest among all the temperatures, resulting in poor photon absorption. Furthermore, η decreases with increasing temperature, from 25.13% at 300 K to 6.04% at 550 K. The InGaN solar cells demonstrated a short-circuit current (I_{sc}) of 39.45 mA/cm^2, an open-circuit voltage (V_{oc}) of 0.7464 V, a maximum power output (P_{max}) of 0.2529 W, a fill factor (FF) of 85.89%, and an efficiency of 25.29%, showing improvements compared to previous works.

1. Introduction

Indium gallium nitride (InGaN) solar cells have a wide operating temperature range, from room temperature to 450 °C, with positive temperature coefficients reaching 350 °C [1]. For example, low indium $In_xGa_{1-x}N$ solar cells with complex architectures have been designed to improve solar cell efficiency (η). However, researchers have reported that as the indium (In) composition increases (more than 20% at room temperature), the increased potential barrier height at the InGaN/gallium nitride (GaN) heterostructure can significantly reduce carrier collection, hence reducing η [2]. Gallium nitride alloys have been found to be favourable for growth on silicon (Si) substrates because of their abundance, non-toxicity, cost-effectiveness, and ease of maintenance, which leads to a relatively low cost per watt of solar cell devices, as mentioned in Ref. [3]. The GaN buffer layer improves crystalline quality, increases electron mobility in the structure, suppresses dislocation propagation, and reduces defect density. The selection of substrate materials is also important in producing high-quality solar cells. Multijunction III-nitride solar cells offer several advantages over Si solar cells, including band gap tunability through elemental composition, higher photon absorption owing to their direct band gap energies, higher resistivity, and lower efficiency degradation due to heat. Moreover, III-nitride materials are cheaper and more cost-effective than raw materials such as Si. In terms of operating temperature, III-nitride materials have excellent temperature tolerance, allowing them to work at both high and low temperatures. Meanwhile, Si solar cells perform poorly at low temperatures due to increased resistivity and

* Corresponding author.
E-mail address: mzmy83@gmail.com

Cite this article as:

Khairuddin, N.S., Mohd Yusoff, M.Z. and Hussin, H.,2026. PC1D Modelling of the Impact of Layer Thickness, Doping Concentration, and Operating Temperature on InGaN Solar Cells. *Progress in Physics of Applied Materials*, *6*(3), pp.193-204. DOI: 10.22075/ppam.2026.39563.1183

can be damaged at higher temperatures. Among the various photovoltaic software programmes available, the Personal Computer One Dimensional (PC1D) simulation was chosen as a simulation tool for this study as it is a user-friendly system. It is also the most widely used and possibly the simplest simulation software. This study proposes a high-efficiency InGaN/GaN solar cell prepared using an Si substrate, with an In composition of x = 0.2, to increase the overall performance of the solar cell.

2. MODELLING AND SIMULATION

Originally, PC1D was developed for Si and conventional group III-V semiconductors. It is user-friendly and freely accessible for researchers to simulate solar cells without the need for fabrication, thereby saving costs and assisting researchers to predict future results. The selection of PC1D software for wide-band-gap nitrides, such as InGaN or GaN, is due to its ability to optimise doping concentration, layer thickness, and temperature, which are important for InGaN solar cells. Auger recombination, Shockley-Read-Hall (SRH) recombination, and band-gap narrowing (BGN) effects are available in PC1D, which are essential for obtaining accurate results for solar cells. The structure consists of an active layer of n-InGaN (0.001 μm) with a doping concentration of 1 × 10^{20} cm^{-3} and a buffer layer of 0.01 μm with a doping concentration of 1 × 10^{19} cm^{-3}. This study proposes an efficient InGaN/GaN solar cell using an Si substrate with a layer thickness of 250 μm and a doping concentration of 1 × 10^{17} cm^{-3} to enhance overall solar cell performance. Figure 1(a) illustrates the schematic construction of the InGaN/GaN/Si heterojunction solar cell, which consists of three layers: n-InGaN, n-GaN, and p-Si as the substrate layer. Figure 1(b) depicts the energy band diagram of the conduction and valence bands of the InGaN/GaN/Si heterojunction solar cell. The band gap is an important term in materials, which refers to the minimum energy required for electrons to move to a higher energy level. The mobility, absorption coefficients, and recombination rates of InGaN and GaN were taken from previous studies [4]. A standard illumination setting of one-sun and AM1.5G solar radiation with a constant intensity of 0.1 W/cm^2 was used to investigate the solar cell performance in PC1D simulation. When the heterojunction device is under illumination, the flat band potential is displaced negatively, altering the depletion layer and affecting device performance. The PC1D solver is widely used in simulating one-dimensional crystalline solar cell devices, allowing for adjustments in various design parameters in solar cells.

To investigate the stability of the geometrical properties of the solar cell, the operating temperature of the optimised parameters was studied at temperatures ranging from 300 K to 550 K. Table 1 lists several electrical and optical parameters, including energy band gap, intrinsic concentration, doping concentration, bulk recombination, dielectric constant, refractive index, and others.

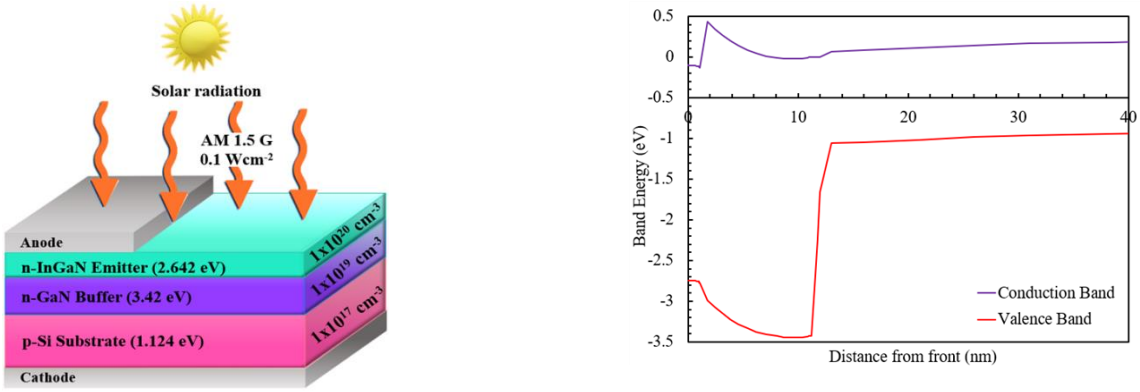

Fig. 1. (a) The three-dimensional schematic device structure and (b) the energy band diagram of the InGaN/GaN/Si solar cell.

Table 1. Simulated variables of the InGaN-based solar cell.

Variables		Value	
Active area		10 cm^2	
Section	n-InGaN	n-GaN	p-Si
Depth	0.001 μm	0.01 μm	250 μm
Band gap	2.6	3.4 eV	1.12 eV
Background doping	1 × 10^{20} cm^{-3}	1 × 10^{19} cm^{-3}	1 × 10^{17} cm^{-3}
Dielectric constant	10.8	8.9	11.9
Refractive index	2.41	2.29	3.58
Excitation mode	One-sun (transient; 16 timesteps)		
Spectrum	AM1.5G		
Intensity	0.1 W/cm^2		

Fig. 2 shows the electron flow in the depletion zone between n-InGaN, n-GaN, and p-Si. When the cell is illuminated, photons with energy exceeding the semiconductor's band gap energy generate electron-hole pairs. During the charge exchange process, the separation of the excess charge carriers takes place in the space charge region. The width of this region is in proportion to the height of the potential barrier. This barrier does not allow the flow of electrons from the metal to the semiconductor, as expressed in Ref. [5]. As the depletion region expands, the bound charges create a potential difference, resulting in the creation of an electric field within the region. These processes are vital for increasing photocurrent output and η.

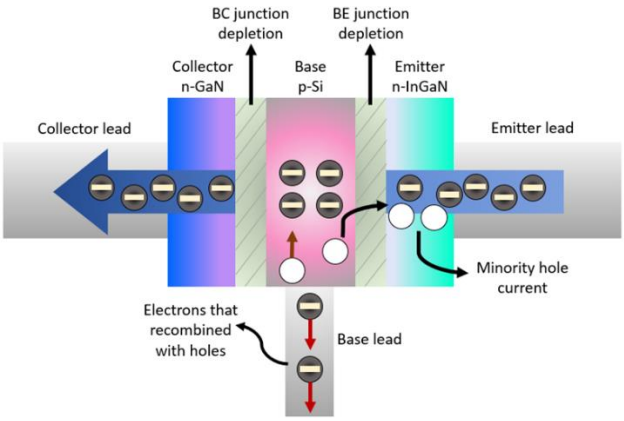

Fig. 2. The depletion region in the InGaN/GaN/Si-based solar cell.

The PC1D models applied in this work are presented in Equations (1) – (7), which are used for optimising the performance of solar cells.

$$J_p = \mu_p . p . \nabla E_{Fp} \quad (1)$$

$$J_n = \mu_n . n . \nabla E_{Fn} \quad (2)$$

where J_n and J_p are the electron and hole current densities, respectively, and n and p are the electron and hole densities, respectively. μ_n and μ_p are the electron and hole mobilities, respectively, and E_{Fn} and E_{Fp} are the diffusion coefficients.

$$\frac{\partial_n}{\partial_t} = \frac{\nabla . J_n}{q} + G_L - U_n \quad (3)$$

$$\frac{\partial_p}{\partial_t} = \frac{\nabla . J_p}{q} + G_L - U_p \quad (4)$$

$$\Delta^2 \phi = \frac{q}{\in}(n - p + N_{acc}^{-} - N_{don}^{+}) \quad (5)$$

Equations (3) and (4) are derived using the conservation of charge or the continuity equation. The generation and recombination rates are assigned as G_L and U_p, respectively. Equation (5) is the Poisson's equation for calculating the electrostatic potential, where N_{acc}^{-} and N_{don}^{+} are the doping concentrations of acceptor and donor elements, respectively.

$$n = N_C F_{1/2}\left(\frac{q\psi + V_n - q\phi_{n,t} + ln(n_{t,0}/N_c)}{k_B T}\right) \quad (6)$$

$$p = N_V F_{1/2}\left(\frac{-q\psi + V_p - q\phi_{p,t} + ln(n_{t,0}/N_V)}{k_B T}\right) \quad (7)$$

By combining three fundamental equations with finite element calculation, the optimum conditions for fabricating solar cells with optimum accuracy can be determined. Different parameters were used to optimise solar cell performance, as presented in Equation (8).

$$\eta = \frac{P_{max}}{I_{in}} = \frac{J_{mpp} V_{mpp}}{I_{in}} = \frac{J_{sc} V_{oc} FF}{I_{in}} \quad (8)$$

where η, P_{max}, and I_{in} are the efficiency, maximum output power, and incident power, respectively. While, J_{mpp} and V_{mpp} are the current and voltage at the maximum power point (MPP). Subsequently, J_{sc}, V_{oc} and FF are short-circuit current, open-circuit voltage, and fill factor, respectively.

3. Results and Discussion

In this initial simulation, the thickness of the InGaN layer was varied from 0.001 µm to 0.04 µm, while the concentration ($1x10^{20}$ cm^{-3}) remained constant across all devices. Figures 3(a)–(d) present the electrical properties of the simulated solar cells. Figure 3(a) shows that the short-circuit current (I_{sc}) decreases as the thickness of the InGaN layer increases. Table 2 indicates that increasing the thickness of the InGaN active layer from 0.001 µm to 0.04 µm leads to lower η. This suggests that changes in the thickness of the InGaN layer affects all cell characteristics. The increased I_{sc} implies that increasing η is directly related to the rate of energy absorption. Moreover, recent studies have reported that the efficiency of solar cells remains unchanged for the p-InGaN thickness between 0.001 µm and 0.01 µm. Due to the limitations of the PC1D software, the thickness of any material modelled on this platform must be at least 0.001 µm and at most 100,000 µm. Other factors, such as a higher In content of InGaN, can adversely affect the efficiency of solar cells [6]. Furthermore, as the thickness of the InGaN layer increases, so does the density of dislocations, which reduces the quality of the layer [7]. The thinnest InGaN active layer, at 1×10^{-3} µm (25.29%), achieved the highest η of layer thickness influence, with V_{oc} = 0.7464 V, I_{sc} = 39.45 mA/cm^2, P_{max} = 0.2529 W, and FF = 85.89%.

The intensity of the photons that pass through the material will be directly affected by the level of doping since the absorbing and transporting properties of the semiconductor will be as indicated in Ref. [8]. Furthermore, it is believed that optimising the doping concentration of the solar cell's active layer may enhance solar spectrum absorption, hence increasing the cell's η.

In the second simulation, the concentration of the InGaN layer was changed, starting at 1×10^{17} cm^{-3} and reaching a maximum of 1×10^{20} cm^{-3}. The thickness of the InGaN layer (0.001 µm) stayed the same for all the devices. In Figure 4(a), the I_{sc} increases from 1×10^{17} cm^{-3}, reaching a peak at 1×10^{20} cm^{-3}, and then decreases as the doping concentration continues to increase. Figure 4(b) shows that the maximum output power does not differ significantly across doping concentrations. Figures 4(c) and 4(d) illustrate that the solar cells' FF and η increase

with increasing InGaN doping concentration, peaking at 1 × 10^{20} cm^{-3} with 85.89% and 25.29%, respectively, before decreasing at 1 × 10^{21} cm^{-3}.

Table 3 shows no significant difference between I_{sc} and V_{oc}; however, both *FF* and η increase with increasing doping concentration, and decrease when doping concentration exceeds 1 × 10^{20} cm^{-3}. At a doping concentration of 1 × 10^{20} cm^{-3}, InGaN doping achieved the maximum η (V_{oc} = 0.7464 V, I_{sc} = 39.45 mA/cm^2, P_{max} = 0.2529 W). For optimal solar cell performance, InGaN doping concentrations must be between 1 × 10^{17} cm^{-3} and 1 × 10^{20} cm^{-3}.

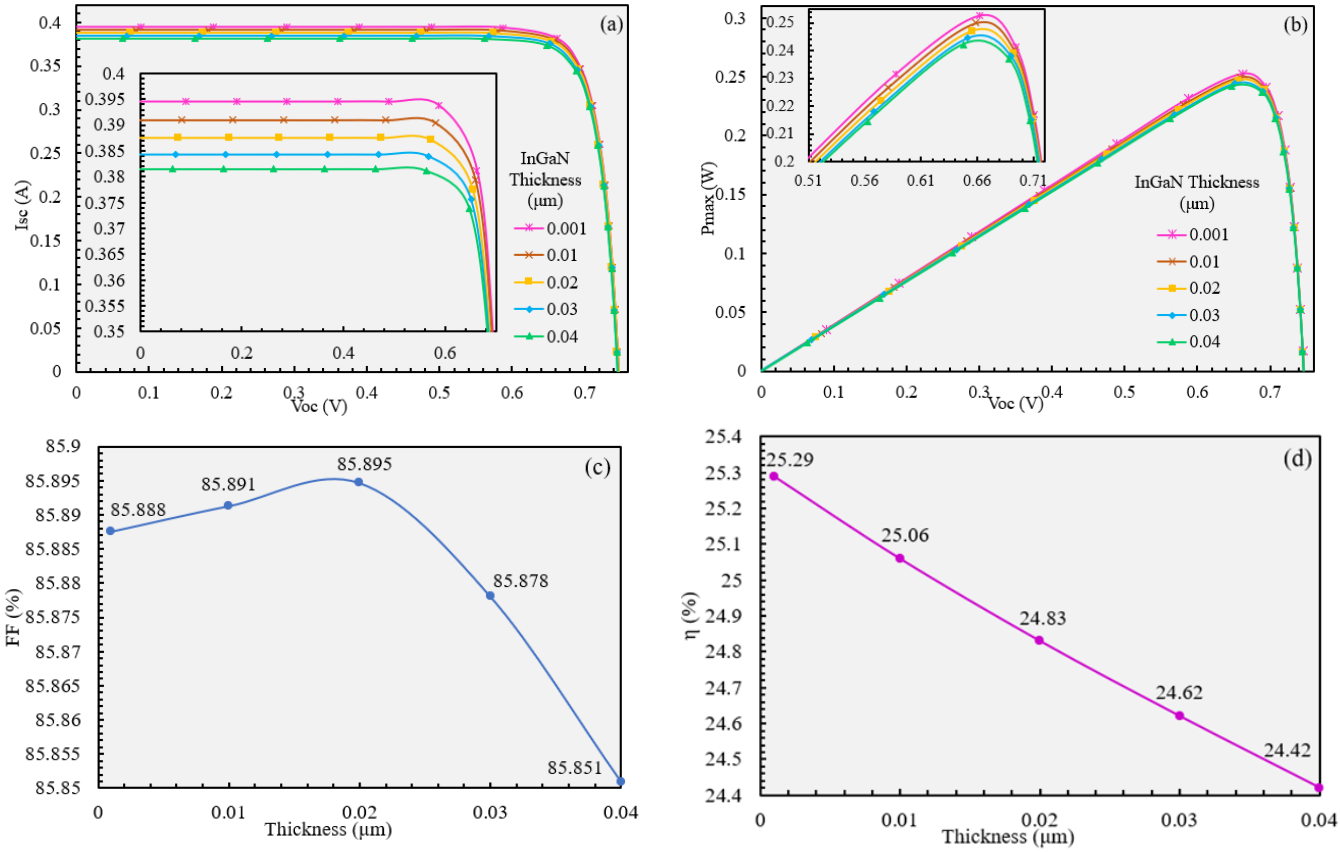

Fig. 3. (a) I–V characteristics, (b) P–V characteristics, (c) *FF*, and (d) η for different InGaN thicknesses.

Table 2. Electrical properties of solar cells in relation to InGaN thickness.

Thickness of n-InGaN (µm)	Short-Circuit Current (A)	Open-Circuit Voltage (V)	Maximum Power (W)	Fill Factor (%)	Efficiency (%)
0.001	0.3945	0.7464	0.2529	85.89	25.29
0.01	0.391	0.7462	0.2506	85.89	25.06
0.02	0.3875	0.746	0.2483	85.87	24.83
0.03	0.3844	0.7458	0.2462	85.88	24.62
0.04	0.3815	0.7456	0.2442	85.85	24.42

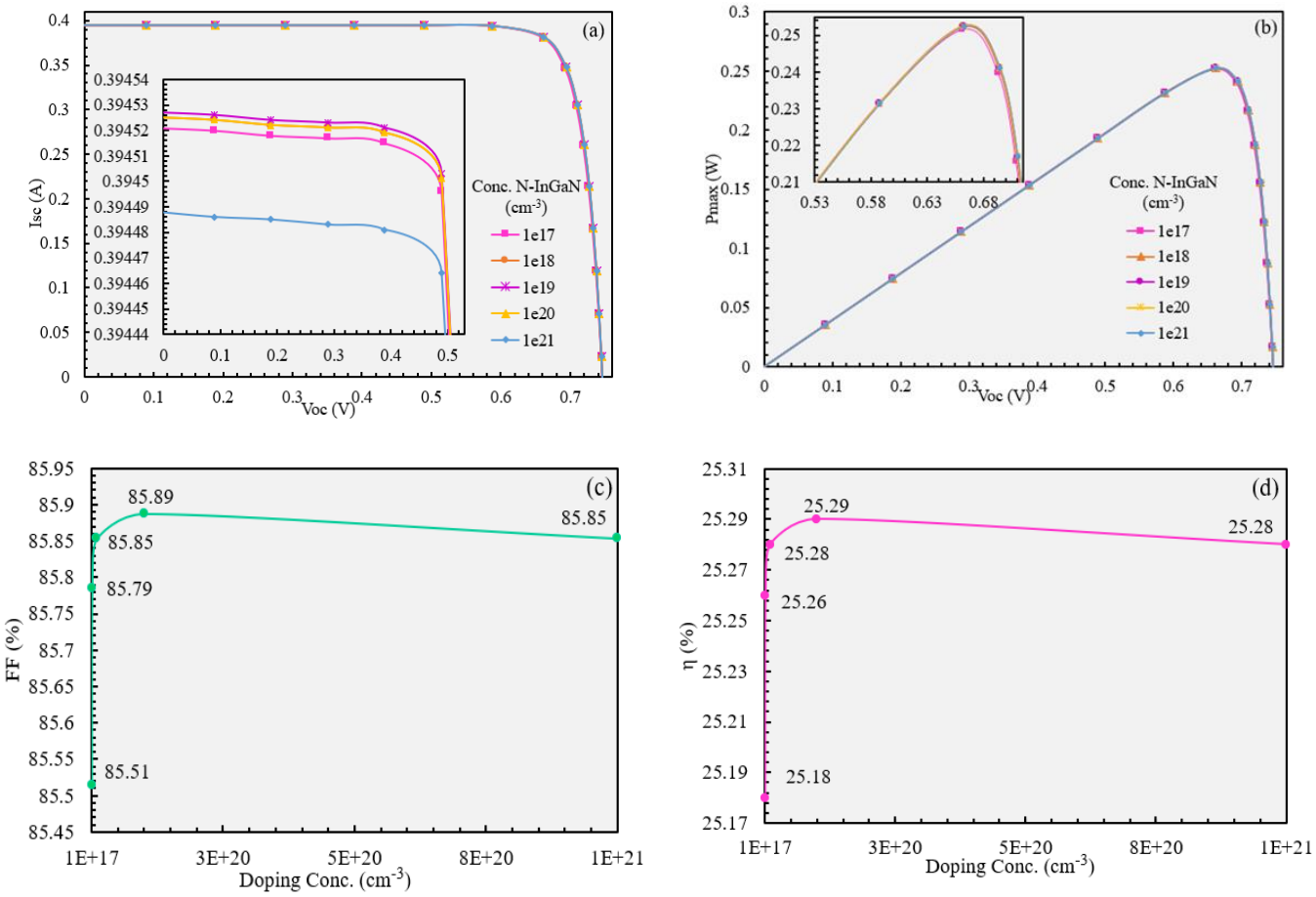

Fig. 4. (a) I–V characteristics, (b) P–V characteristics, (c) *FF*, and (d) η for different n-type InGaN concentrations.

Table 3. *J-V* parameters of experimental and simulated outcomes.

N-InGaN Dop. Conc. (cm^{-3})	Short-Circuit Current (A)	Open-Circuit Voltage (V)	Maximum Power (W)	Fill Factor (%)	Efficiency (%)
1×10^{17}	0.3945	0.7464	0.2518	85.51	25.18
1×10^{18}	0.3945	0.7464	0.2526	85.79	25.26
1×10^{19}	0.3945	0.7464	0.2528	85.85	25.28
1×10^{20}	0.3945	0.7464	0.2529	85.89	25.29
1×10^{21}	0.3945	0.7464	0.2528	85.85	25.28

The presence of dislocation density in InGaN solar cells reduces the V_{oc}, I_{sc}, and η. These effects can be attributed to dislocations acting as non-radiative recombination centres, which increase the probability of electron-hole pair recombination after exposure to illumination [9]. The thickness of the InGaN layer is vital in determining the solar cell performance. An increase in InGaN thickness can lead to the formation of dislocation loops, which degrade the intensity of photoluminescence and the performance of solar devices [10]. Moreover, several processes can explain why electron mobility increases at high doping concentrations. One of them is the reduction of scattering effects, where a high doping concentration reduces the scattering of charge carriers, and the free carriers from the dopants reduce the scattering effects from impurities and defects [11]. It has been suggested that higher doping concentrations can enhance electron conductivity and mobility as they have more option to move into the material [12].

This study used various thicknesses of InGaN for the simulation, starting from 0.001 µm to 0.04 µm. As shown in Table 2, the efficiencies for 0.001 µm and 0.01 µm are almost identical, which increase as the thickness increases. This can be explained by the fact that increasing the InGaN thickness may lead to dislocations, which reduce the photointensity and device performance [10]. A similar trend was observed for doping, where the doping rate ranges from 10^{17} to 10^{18} cm^{-3}. However, according to Table 3, the doping concentrations of 1×10^{20} cm^{-3} for InGaN and 1×10^{19} cm^{-3} for GaN exhibit nearly the same efficiency and show an insignificant difference with other devices with lower doping concentrations.

Building a junction using large band gap materials reduces surface recombination and allows solar energy to reach the Si depletion region, hence reducing carrier loss [13]. The principal function of a buffer layer in a heterojunction is to form a junction with the absorber layer while allowing the spectrum to pass through to the junction region and absorber layer.

In the third simulation, the thickness of the GaN layer was changed, starting from 0.01 μm to 20 μm. The concentration of the GaN layer (1x10^{19} cm^{-3}) stayed the same for all the devices. Figure 5 displays the device performance for all parameters. As the thickness of the GaN buffer layer increases, the I_{sc} decreases but the P_{max} does not change significantly. The highest percentage of *FF* was observed at 5 μm, and the percentage decreases gradually as the thickness of the GaN layer increases. The thinnest layer (0.001 μm) exhibits the highest peak η, which declines with increasing layer thickness.

As the thickness of the GaN layer increases, the percentage of external quantum efficiency (EQE) decreases and the absorption range shortens. A wide range of solar spectrum absorption is necessary to improve η. A thin GaN buffer layer enables the solar cell to absorb a long-range wavelength spectrum (middle UV to near IR), thus increasing η and improving cell performance. The thinnest GaN buffer layer (0.01 μm) achieved the highest η of 25.29%, with V_{oc} = 0.7464 V, I_{sc} = 39.45 mA/cm^2, P_{max} = 0.2529 W, and *FF* = 85.89%.

The impact of various doping concentrations on the GaN buffer layer is examined to understand their effects on the solar cells' η. In the fourth simulation, the concentration of the GaN layer was changed, starting at 1 × 10^{15} cm^{-3} and reaching a maximum of 1 × 10^{19} cm^{-3}. The thickness of the GaN layer (0.01 μm) remained the same for all the devices.

As shown in Figures 6(a) and 6(b), the I_{sc} and P_{max} do not differ significantly; however, the *FF* (in Figure 6(c)) and the η (in Figure 6(d)) increase with higher doping concentrations in the GaN buffer layer. An approach to improve solar cell efficiency is to increase the V_{oc} by increasing the dopant concentration. However, this approach can lead to an increase in electron-hole pair recombination in highly doped regions. High doping concentrations in the buffer layer are necessary to absorb most of the solar spectrum, thereby reducing surface recombination and increasing electron mobility into the substrate layer. Table 5 presents the electrical properties of various doping concentrations in the n-GaN buffer layer. The modification of the doping concentration can be utilised to illustrate the electron mobility and η of the solar cells. However, excessive doping in this layer decreases the solar cell's reverse saturation current, hence increasing the V_{oc}.

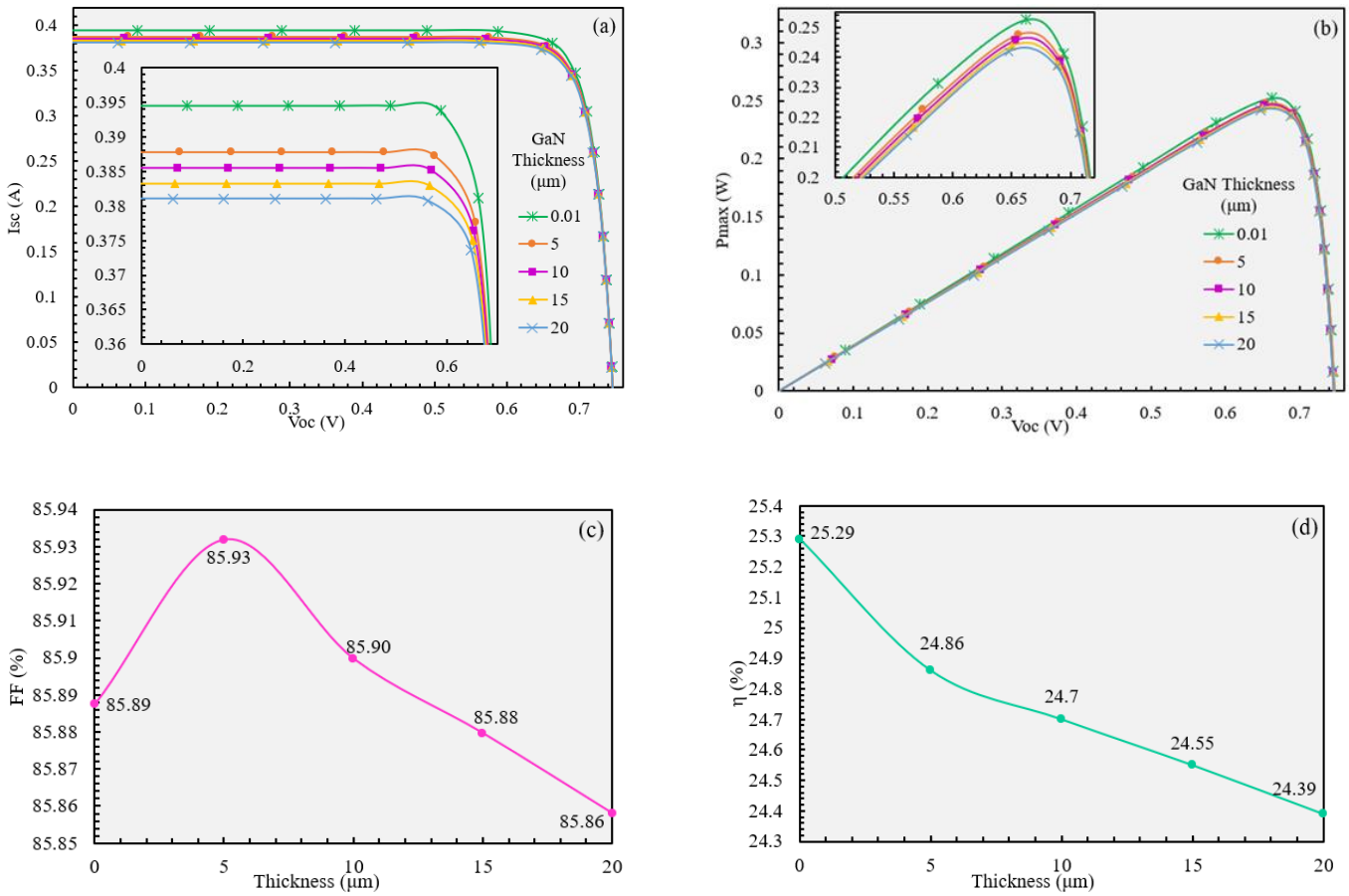

Fig. 5. (a) I–V characteristics, (b) P–V characteristics, (c) *FF*, and (d) η for different GaN thicknesses.

Table 4. Electrical properties of solar cells in relation to GaN thickness.

Thickness of n-GaN (μm)	Short-Circuit Current (A)	Open-Circuit Voltage (V)	Maximum Power (W)	Fill Factor (%)	Efficiency (%)
0.0l	0.3945	0.7464	0.2529	85.89	25.29
5	0.3878	0.746	0.2486	85.93	24.86
10	0.3855	0.7459	0.247	85.89	24.7
15	0.3833	0.7458	0.2455	85.87	24.55
20	0.381	0.7456	0.2439	85.85	24.39

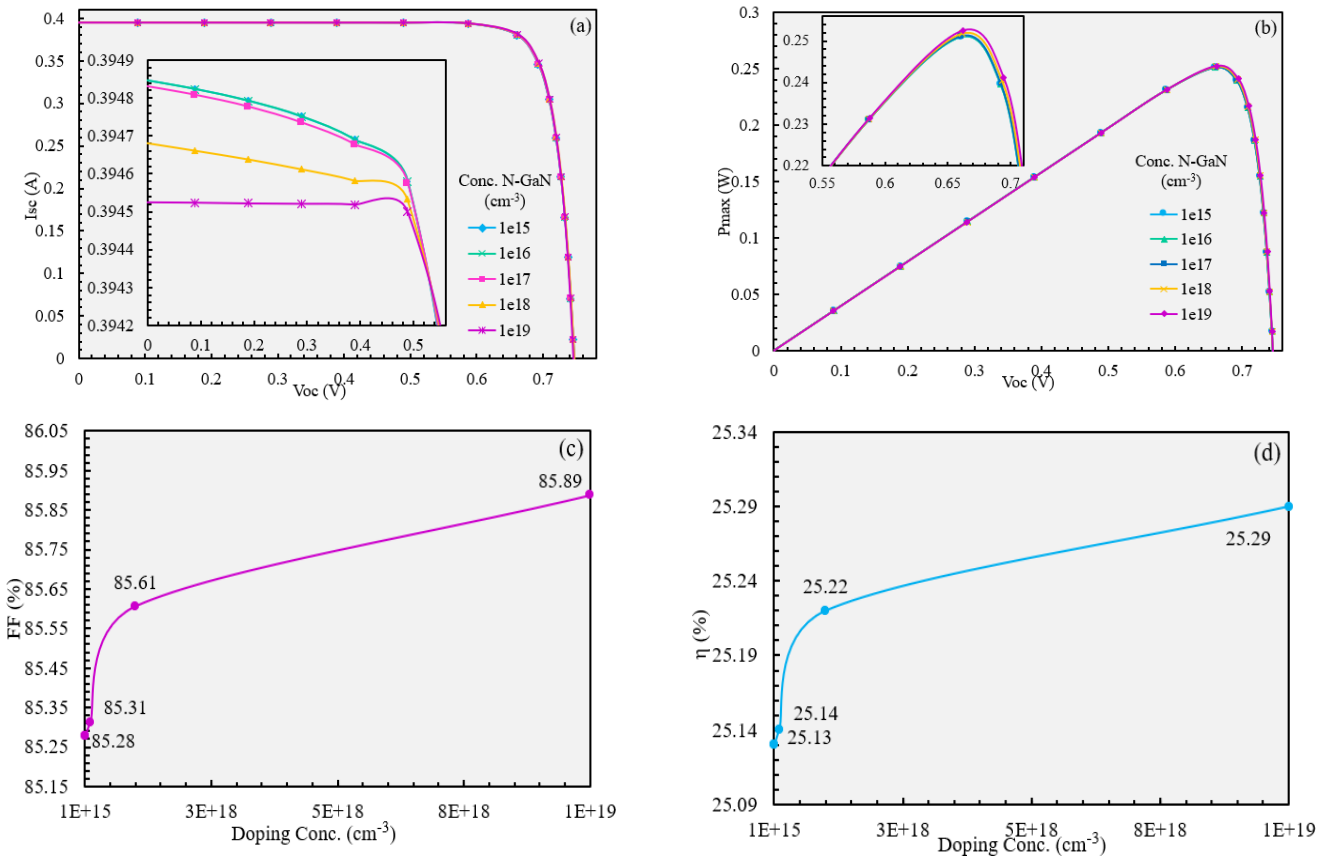

Fig. 6. (a) I–V characteristics, (b) P–V characteristics, (c) *FF*, and (d) η for different n-type GaN concentrations.

Table 5. Electrical properties of solar cells in relation to GaN concentration.

N-GaN Dop. Conc. (cm^{-3})	Short-Circuit Current (A)	Open-Circuit Voltage (V)	Maximum Power (W)	Fill Factor (%)	Efficiency (%)
1×10^{15}	0.3948	0.7464	0.2513	85.28	25.13
1×10^{16}	0.3948	0.7464	0.2513	85.28	25.13
1×10^{17}	0.3948	0.7464	0.2514	85.31	25.14
1×10^{18}	0.3947	0.7464	0.2522	85.61	25.22
1×10^{19}	0.3945	0.7464	0.2529	85.89	25.29

In the fifth simulation, the thickness of the Si base layer was varied between 100 μm and 300 μm. The concentration of the Si base layer ($1x10^{17}$ cm^{-3}) remained the same for all the devices. The thickness of the Si base layer of the solar cell was varied between 100 μm and 300 μm to study the effect of substrate changes. The thickness of the Si substrate layer of 300 μm produced the highest current value, whereas 100 μm resulted in the lowest one, as shown in Figure 7(a). Figures 7(b) and 7(c) show that the I_{sc} and P_{max} increase with layer thickness, with the maximum *FF* (86.16%) obtained at 150 μm. Furthermore, Figure 7(d) depicts how efficiency varies with changes in Si layer thickness. The highest η (25.29%) was observed at 250 μm, decreasing as the Si layer thickness exceeds this value.

Furthermore, as the layer thickness increases, more photons are absorbed; however, carrier mobility decreases due to higher contaminants [14]. Table 6 indicates that the effectiveness of Si substrates increases with increasing layer thickness but decreases beyond 250 µm. The increase in substrate layer thickness gradually enhances η. The highest η was achieved at 250 µm (25.29%), with I_{sc} = 39.45 mA/cm^2, V_{oc} = 0.7464, P_{max} = 0.2529 W, and FF = 85.89%.

In the sixth simulation, the concentration of the Si substrate layer was changed, starting at 1 × 10^{14} cm^{-3} and reaching a maximum of 1 × 10^{18} cm^{-3}. The thickness of the Si substrate layer (250 µm) continued the same for all the devices. Figure 8 depicts the effect of varying Si substrate concentrations on the electrical properties of the solar cells. Both I_{sc} and P_{max} decrease as the doping concentration of the Si substrate increases. Furthermore, increasing the doping concentration of the substrate elevates the rate closer to the interface, leading to a reduction in η. The electrical properties for different Si doping concentrations show that P_{max}, FF, and η improve as the doping concentration increases from 1 × 10^{14} cm^{-3} to 1 × 10^{17} cm^{-3}, but decline at 1 × 10^{18} cm^{-3}. The I_{sc} and V_{oc} exhibit no significant differences (refer to Table 7). The optimal parameters (1 × 10^{17} cm^{-3}) are obtained at V_{oc} = 0.7464 V, I_{sc} = 39.45 mA/cm^2, P_{max} = 0.2529 W, and FF = 85.89%.

In the seventh simulation, the temperature of the device was changed, starting at 300 K and reaching a maximum of 550 K. The thickness and concentration of the device stayed the same for all the operating temperatures. As the temperature increases, the intrinsic carrier concentration increases because the higher temperature provides more energy for electrons to jump from the valence band to the conduction band, thus increasing the number of free charge carriers [15, 16]. The band gap of a semiconductor narrows as the temperature increases, a phenomenon known as BGN. This occurs because the increased thermal energy causes lattice vibrations that affect the band structure [15]. At high temperatures, Auger and SRH recombination processes have a more significant impact on solar cell performance. These processes are related to charge carriers and defects in the material [17, 18].

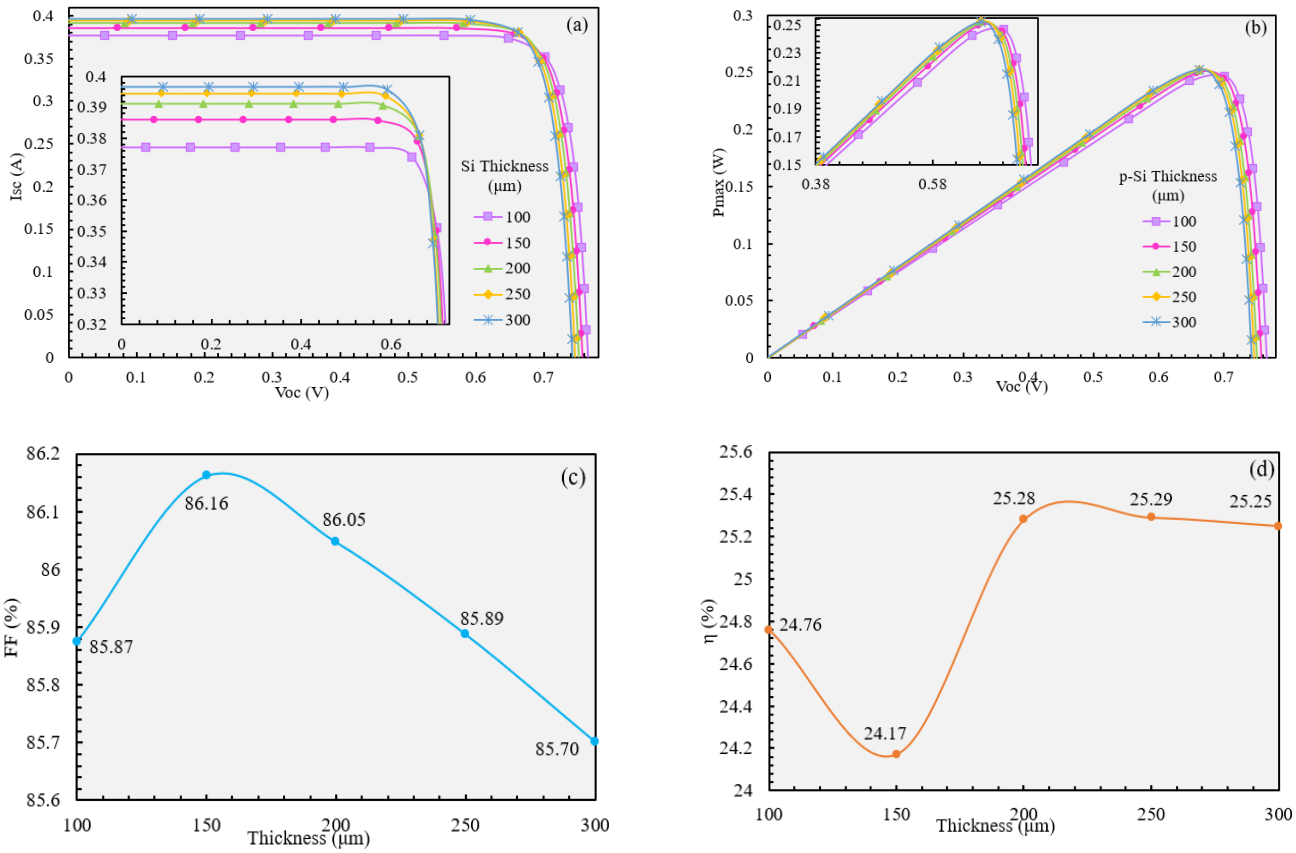

Fig. 7. (a) I–V characteristics, (b) P–V characteristics, (c) *FF*, and (d) η for different p-type Si thicknesses.

Table 6. Electrical properties of solar cells in relation to Si thickness.

Thickness of p-Si (µm)	Short-Circuit Current (A)	Open-Circuit Voltage (V)	Maximum Power (W)	Fill Factor (%)	Efficiency (%)
100	0.377	0.7648	0.2476	85.87	24.76
150	0.386	0.7568	0.2417	86.16	24.17
200	0.3912	0.751	0.2528	86.05	25.28
250	0.3945	0.7464	0.2529	85.89	25.29
300	0.3967	0.7427	0.2525	85.7	25.25

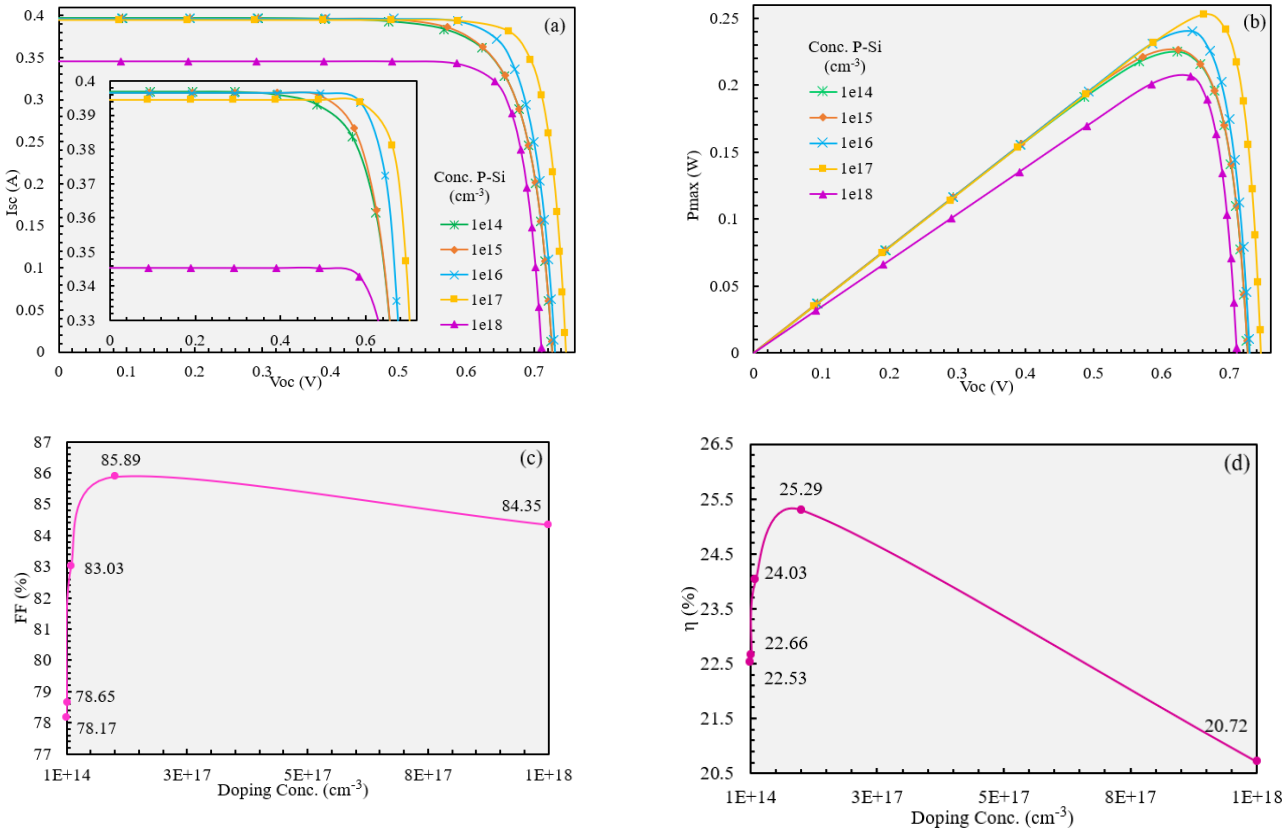

Fig. 8. (a) I–V characteristics, (b) P–V characteristics, (c) *FF*, and (d) η for different p-type Si concentrations.

Table 7. Electrical properties of solar cells in relation to Si concentration.

P-Si Dop. Conc. (cm^{-3})	Short-Circuit Current (A)	Open-Circuit Voltage (V)	Maximum Power (W)	Fill Factor (%)	Efficiency (%)
1×10^{14}	0.3969	0.7262	0.2253	78.17	22.53
1×10^{15}	0.3966	0.7265	0.2266	78.64	22.66
1×10^{16}	0.3964	0.7301	0.2403	83.03	24.03
1×10^{17}	0.3945	0.7464	0.2529	85.89	25.29
1×10^{18}	0.3454	0.7112	0.2072	84.35	20.72

To determine the best performance of a solar cell, we simulated its behaviour at several operating temperatures. The performance of a solar cell can be assessed in terms of I_{sc}, V_{oc}, and P_{max}, whereas the I–V and P–V curves can be used to compute *FF* and η. Figures 9(a) and 9(b) show that the I_{sc} does not change significantly across temperatures; however, both V_{oc} and P_{max} decrease as the operating temperature increases. The reduction in V_{oc} with increasing operating temperature leads to an increase in the density of surface defects, resulting in a high junction resistance. Figures 9(c) and 9(d) indicate that as the operating temperature rises from 300 K to 550 K, both *FF* and η decrease. Consequently, lowering the operating temperature increases the density of surface imperfections, which increases resistance and decreases V_{oc} and I_{sc} [19]. Figure 10 depicts the effect of various operating temperatures on the quantum efficiency (QE) of photovoltaic (PV) solar cells. The QE value at the highest temperature (550 K) is the lowest among all temperatures, indicating insufficient photon absorption. Table 8 shows that there is no significant variation in I_{sc} (0.39 A), while V_{oc}, P_{max}, and *FF* decrease with increasing temperature. The η declines as the temperature rises, from 25.13% (300 K) to 6.04% (550 K).

Fig. 11 illustrates the electrical properties of the solar cells. The optimum point of (I_p, V_p) is determined as (0.38, 0.66). The simulated solar cell achieved its maximum η at 25 °C, with V_{oc} = 0.7464 V, I_{sc} = 39.45 mA/cm^2, P_{max} = 0.2529 W, η = 25.29%, and *FF* = 85.89%. Several reports using different In fractions for InGaN show efficiency results comparable to the current study [6, 20, 21]. Moreover, our findings are comparable to the very recent studies [6].

Table 9 summarises the literature results for optimised solar cells in comparison with this research. It is evident that our simulated results are significantly higher than both the experimental and simulation results, indicating that our

proposed design and parameters are suitable for fabricating a high-efficiency solar cell. In the future, we would like to incorporate our InGaN solar cells with multi-layers antireflective coating consisting of MgF_2 & SiO_2 [26], as we thought that the multi-layers ARC would help in reducing the reflection as well as increase the efficiency and performance of solar cells.

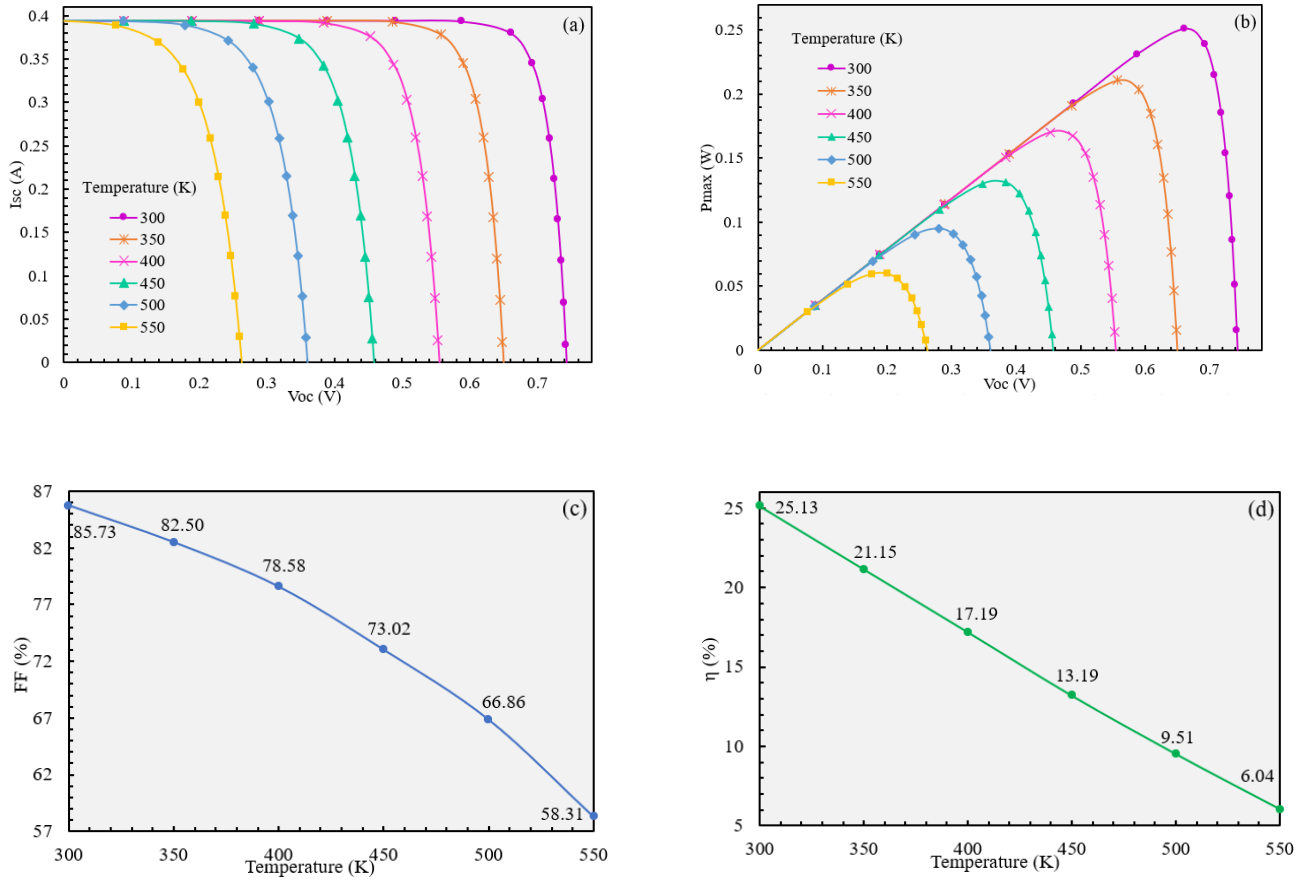

Fig. 9. (a) I–V characteristics, (b) P–V characteristics, (c) *FF*, and (d) η for different operating temperatures.

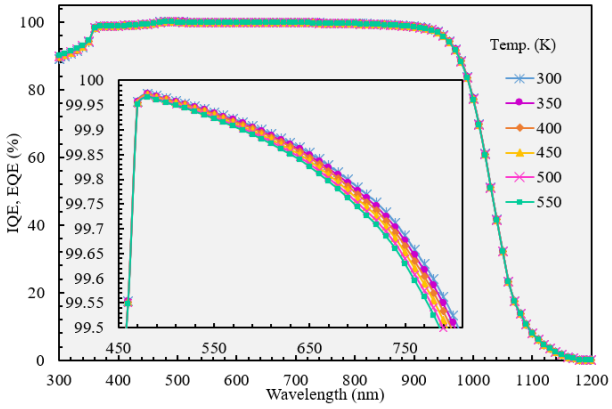

Fig. 10. The EQE under various operating conditions.

Table 8. Electrical properties of solar cells in relation to temperature changes.

Temperature (K)	Short-Circuit Current (A)	Open-Circuit Voltage (V)	Maximum Power (W)	Fill Factor (%)	Efficiency (%)
300	0.3945	0.743	0.2513	0.857347	25.13
350	0.3946	0.6497	0.2115	0.824974	21.15
400	0.3945	0.5545	0.1719	0.785828	17.19
450	0.3943	0.4581	0.1319	0.730227	13.19
500	0.3942	0.3608	0.0951	0.668648	9.51
550	0.3937	0.2631	0.0604	0.58311	6.04

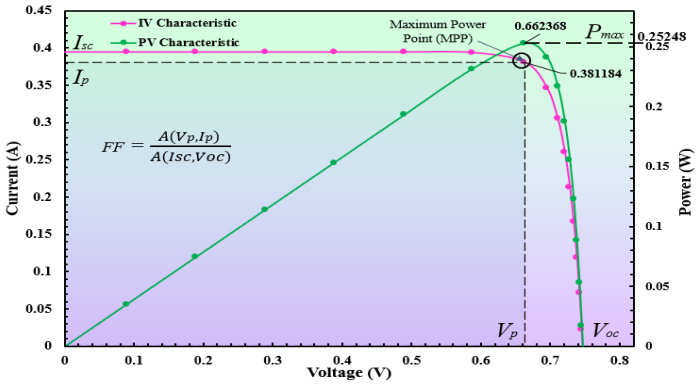

Fig. 11. Electrical properties of solar cell devices.

Table 9. Comparison of literature results for optimised solar cells with this work.

Device Structure	*Jsc* (mA/cm²)	*Voc* (V)	*FF* (%)	*η* (%)	References
InGaN/Si	10.01	1.69	59.12	15	[22]
$In_{0.62}Ga_{0.38}N$	33.57	0.912	87.51	19.8	[23]
$In_{0.07}Ga_{0.93}N$	0.164	2.38	72.25	28	[24]
$In_{0.2}Ga_{0.8}N$	36.9	0.71	84.83	22.1	[25]
InGaN/GaN/Si	39.45	0.746	85.89	25.29	This work

4. Conclusions

In this study, a heterojunction solar cell structure comprising n-InGaN/n-GaN/p-Si was developed using PC1D simulation software, with an In composition of x = 0.2. Utilising PC1D allows for a reduction in costs and expensive instrumentation time during the production process, while also generating reliable data for solar cell research. We have demonstrated that the parameters utilised in this study can enhance performance and identify the maximum η of a solar cell. Adjusting the layer thickness and doping concentration of the InGaN active layer improves solar absorption. Meanwhile, the GaN buffer layer optimises light transmission and increases electron mobility to the substrate. The optimised parameters showed that the optimal PV solar cell performance achieved the highest η of 25.29% with *FF* = 85.89% at room temperature (25 °C), V_{oc} = 0.75 V, I_{sc} = 0.39 A, and P_{max} = 0.253 W.

Funding Statement

This research received no specific grant from any funding agency.

Conflicts of interest

The authors declare that they have no known competing financial interests or personal relationships that could have appeared to influence the work reported in this paper.

Authors contribution statement

Conceptualization and study design: N.S. Khairuddin and M.Z.M. Yusoff, Data collection and experimentation: N.S. Khairuddin, Data analysis and interpretation: N.S. Khairuddin and H. Hussin, Manuscript writing and editing: N.S. Khairuddin, M.Z.M. Yusoff, and H. Hussin**,** Supervision and project administration: M.Z.M. Yusoff and H. Hussin.

References

[1] Yue, Z., Xiang, G., Zhang, J., Zhang, X., Song, C., Ding, B. et al., 2024. Low current driven bidirectional violet light emitting diode based on p-GaN/n-InN heterojunction. *Journal of Luminescence*, 266, p.120295.

[2] Chouchen, B., Ducroquet, F., Nasr, S., Alzahrani, A.Y., Hajjiah, A.T. and Gazzah, M.H., 2022. InxGa1−xN/GaN double heterojunction solar cell optimization for high temperature operation. *Solar Energy Materials and Solar Cells*, 234, p.111446.

[3] Dada, M. and Popoola, P., 2023. Recent advances in solar photovoltaic materials and systems for energy storage applications: A review. *Beni-Suef University Journal of Basic and Applied Sciences*, 12, pp.1–15.

[4] Khairuddin, N.S., Yusoff, M.M. and Hussin, H., 2023. The effects of thickness and doping concentration on the solar efficiency of GaN/p-Si based solar cells. *Chalcogenide Letters*, 20, pp.629–637.

[5] Hijjawi, U., Lakshminarayana, S., Xu, T., Fierro, G.P.M. and Rahman, M., 2023. A review of automated solar photovoltaic

defect detection systems: Approaches, challenges, and future orientations. *Solar Energy*, 266, p.112186.

[6] Wei, Z., Al-Nuaimi, N. and Gemming, S., 2025. Optimization of InGaN-based solar cells by numerical simulation: Enhanced efficiency and performance analysis. *Next Materials*, 6, p.100325.

[7] Zumahi, S.A.A., Basher, M.K., Arobi, N., Rahman, M.M., Tawfeek, A.M., Akand, M.R. et al., 2024. High-efficiency silicon solar cells designed on experimentally achieved nano-engineered low-reflective silicon surface. *Journal of Optics*, pp.1–15.

[8] Armakavicius, N., Knight, S., Kühne, P., Stanishev, V., Tran, D.Q., Richter, S. et al., 2024. Electron effective mass in GaN revisited: New insights from terahertz and mid-infrared optical Hall effect. *APL Materials*, 12, p.021114.

[9] Linkai, Y., Haoran, Q., Jialin, H., Mei, Z., Degang, Z., Desheng, J. et al., 2018. Influence of dislocation density and carbon impurities in i-GaN layer on the performance of Schottky barrier ultraviolet photodetectors. *Materials Research Express*, 5, p.046207.

[10] Faleev, N., Jampana, B., Jani, O., Yu, H., Opila, R., Ferguson, I. and Honsberg, C., 2009. Correlation of crystalline defects with photoluminescence of InGaN layers. *Applied Physics Letters*, 95, p.051914.

[11] Bronger, T. and Carius, R., 2007. Carrier mobilities in microcrystalline silicon films. *Thin Solid Films*, 515, pp.7486–7489.

[12] Das, D. and Patra, C., 2023. Superior phosphorous doping in nanocrystalline silicon thin films and their application as emitter layers in silicon heterojunction solar cells. *Energy & Fuels*, 37, pp.6062–6077.

[13] Wu, N., Xing, Z., Li, S., Luo, L., Zeng, F. and Li, G., 2023. GaN-based power high-electron-mobility transistors on Si substrates: From materials to devices. *Semiconductor Science and Technology*, 38, p.063002.

[14] Danladi, E., Egbugha, A.C., Obasi, R.C., Tasie, N.N., Achem, C.U., Haruna, I.S. and Ezeh, L.O., 2023. Defect and doping concentration study with series and shunt resistance influence on graphene modified perovskite solar cell: A numerical investigation in SCAPS-1D framework. *Journal of the Indian Chemical Society*, 100, p.101001.

[15] Tiandho, Y., Sunanda, W., Afriani, F., Indriawati, A. and Handayani, T.P., 2018. Accurate model for temperature dependence of solar cell performance according to phonon energy correction. *Latvian Journal of Physics and Technical Sciences*, 55, pp.15–25.

[16] Song, J.J., Zhang, H.M., Hu, H.Y., Dai, X.Y. and Xuan, R.X., 2011. Intrinsic carrier concentration in strained Si1−xGex/(101)Si. *Materials Science Forum*, 663, pp.470–472.

[17] Lock, D., Sweeney, S.J., Adams, A.R. and Robbins, D.J., 2003. Auger recombination in InGaAs/AlGaAs-based MQW semiconductor lasers emitting at 980 nm. *Physica Status Solidi (b)*, 235, pp.542–546.

[18] Tanaka, K. and Kato, M., 2024. Carrier recombination in highly Al-doped 4H-SiC: Dependence on the injection conditions. *Japanese Journal of Applied Physics*, 63, p.011002.

[19] Ming, C., Zhou, H., Wu, J., Hu, C., Fan, W., Ma, X. et al., 2023. The design and performance optimization of all-inorganic $CsPbIBr_2/CsSnI_3$ heterojunction perovskite solar cells. *Solar Energy*, 263, p.111885.

[20] Marouf, Y., Dehimi, L., Bouzid, F., Pezzimenti, F. and Della Corte, F.G., 2018. Theoretical design and performance of InxGa1−xN single junction solar cell. *Optik*, 163, pp.22–32.

[21] Adaine, A., Hamady, S.O.S. and Fressengeas, N., 2016. Simulation study of a new InGaN p-layer free Schottky based solar cell. *Superlattices and Microstructures*, 96, pp.121–133.

[22] Ghosh, B.K., Mohamad, K.A., Saad, I. and Zainal, S.S.M., 2014. Performance analysis based on different indium content for InGaN/Si heterojunction solar cell. *Proceedings of the 3rd IET International Conference on Clean Energy and Technology (CEAT 2014)*, p.33.

[23] Nour, S., Merabti, A., Issani, H., Abdeldjebar, R. and Djatout, A., 2023. Optimization the characteristics of solar cell based on InGaN. *Turkish Journal of Computer and Mathematics Education*, 14, pp.1–9.

[24] Shan, H.S., Li, X.Y., Chen, B., Ma, S.F., Li, L. and Xu, B.S., 2019. Effect of indium composition on the microstructural properties and performance of InGaN/GaN MQWs solar cells. *IEEE Access*, 7, pp.182573–182579.

[25] Bouadia, A., Naima, H., Djelloulc, A., Benkrimad, Y. and Farese, R., 2022. Enhancing the efficiency of the gallium indium nitride (InGaN) solar cell by optimizing the effective parameters. *Chalcogenide Letters*, 19, pp.611–619.

[26] Salmaniannezhad, H., Salmaniannezhad, H., Zarei Moghadam, R., Khani, M., Ardani, M. and Shokri, B., 2023. Design and fabrication of multi-layers antireflection coating consisting of MgF_2 and SiO_2. *Progress in Physics of Applied Materials*, 3(2), pp.141-146.